USGS Award Number G18AP00008

# Time-dependent Model and Underlying Mechanism of Creep Rate Variations on the Hayward Fault

Manoochehr Shirzaei
Arizona State University, Tempe, Az, 85287

Phone: 4807274193
Fax: 4809658102
Duration: 01/01/2018-12/30/2019

## 1. Introduction

Within the earthquake cycle, fault slip comprises seismic and aseismic components, which are believed to occur on patches with velocity weakening (VW) and velocity strengthening (VS) properties [*Dieterich*, 1978; *Ruina*, 1983] (Fig. 1). Understanding, why, when, where, and how aseismic slip (or creep) varies on a fault is essential for quantifying earthquake potential [*Avouac*, 2015]. Creep plays a crucial role in the earthquake cycle and can account for more than half of the seismic moment budget in the seismogenic zone [Pacheco et al., 1993]. The spatial distributions of creep provide information on the extent to which the plate interface is locked [*Chlieh et al.*, 2014; *Perfettini et al.*, 2010] and also allows estimating location and size of future earthquakes [*Kawasaki et al.*, 2001]. On the other hand, the temporal variation in the extent and rate of creep can be used to determine fault frictional properties [*Perfettini et al.*, 2010; *Shirzaei et al.*, 2014; *Wallace et al.*, 2012] and has implications for earthquake rupture nucleation, triggering, and termination [*Cho et al.*, 2009]. More recently it has been suggested that propagation of creep in the form of slow slip events can precede earthquakes, such as the Mw 9.0, 11th March 2011, Tohoku earthquake [*Kato et al.*, 2012; *Uchida et al.*, 2016], the Mw 8.1, 1st April 2014, Iquique earthquake [*Schurr et al.*, 2014] and the Mw 7.3, 18 April 2014 Papano earthquake [*Radiguet et al.*, 2016]. These observations suggest that fault creep plays an essential role in determining the overall earthquake patterns and that the frictional properties of faults are variable spatially. Noteworthy, numerical studies indicate that the extent, size and timing of earthquakes are determined by the frictional properties of the fault interface [*Kaneko et al.*, 2010].

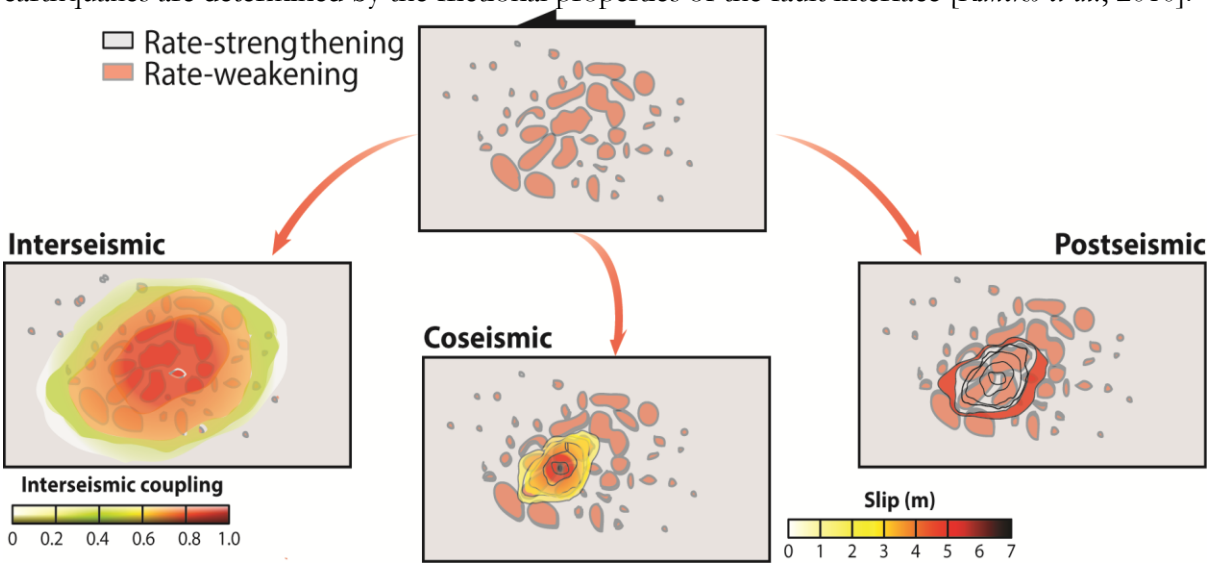


**Figure 1.** Conceptual model of the earthquake cycle (modified from *Avouac* [2015]). It shows how the pattern of VW vs. VS zones may vary on fault and how geodetically-derived interseismic coupling models gives only a first-order estimate of VW and VS zones. This pattern will also determine the patterns of interseismic coupling, seismic ruptures, and afterslip.

**Here we measured spatially and temporally variable creep rates on the Hayward Fault (HF) and Rodgers Creek Fault (RCF) through kinematic models that integrate geodetic and seismic observations. To this end, we have analyzed a large set of SAR data acquired by Sentinel-1A/B satellites through an advanced multitemporal interferometric processing. Our kinematic model suggests that Hayward fault alone accumulates an equivalent seismic moment of 5.2 – 5.5 each year. This estimate for Rodgers Creek Fault is 5.0 – 5.4, while the combined system collects a moment at the rate of 5.4 – 5.7 per year.**

## 2. Background

The Hayward fault, extending for about ~70 km onshore of the eastern San Francisco Bay area, accommodates ~25% of the relative motion between the Pacific and the Sierra Nevada – Great Valley plates [*d'Alessio et al.*, 2005] (Fig. 2A). In the past, this fault has shown distinct phases of activity, including large coseismic ruptures (such as a ~Mw 6.8 earthquake in 1868), frequent microseismicity, and aseismic creep [*Lienkaemper et al.*, 1991; *Toppozada and Borchardt*, 1998]. The northern extension of the HF, namely Rodgers Creek Fault (Fig. 2A), also hosted moderate magnitude $M_L$ 5.6 and $M_L$ 5.7 in 1969 near the city of Santa Rosa, located on the central part of the fault. Within the next 30 years, there is a ~32% likelihood for an $M_w$ 6.7+ earthquake on Hayward-Rodgers Creek Fault [*Field et al.*, 2015]. Moreover, relying on paleoseismic observations, 1900-yr earthquake chronology of the 12 most recent earthquakes, *Lienkaemper et al.* [2010] determined a 161 ± 65 yr mean recurrence interval and suggested a ~29% (±6%) chance for a large event by 2040. Using a frictional model, *Savage and Lisowski* [1993] relate the surface creep rate to the rate of stress accumulation and estimated a strain accumulation rate equivalent to an Mw 6.8 event per century on HF alone. Considering a bigger fault rupture area, *Lienkaemper and Galehouse* [1998] doubled the estimate of the HF seismic potential. Also, a recent study based on subsurface imaging and geophysical observation suggests that HF and RCF are connected beneath San Pablo Bay, which means that this fault has the potential to generate significant earthquakes as large as Mw 7.4 [*Watt et al.*, 2016].

Surface creep observed along the full 70-km-long onshore extent of the HF. Given the long-term slip rate of 9 ± 2 mm/yr, 30-90% of this rate is accommodated by aseismic creep at the surface [*Lienkaemper et al.*, 1991; *Lienkaemper et al.*, 1997]. Using GPS data and two ERS interferograms, *Bürgmann et al.* [2000] estimate that ~7 mm/yr creep extends to nearly the base of the seismogenic zone along the northern ~20 km and southern ~10 km of the HF. Also, *Evans et al.* [2012] inverted for regional fault slip rates and distributed creep on the HF, relying on a block model approach. Their geodetic long-term slip rate estimate is 6.7±0.8 mm/yr, and the creep rates generally increase with depth. Using boundary-element models of a stress-free shallow fault driven by slip below the seismogenic zone, *Simpson et al.* [2001] find that creep reaches to depths of 4-12 km on the Hayward Fault. However, using a local recurrence-time method based on the size-frequency distribution of micro-earthquakes, *Wyss* [2001] identified a central locked asperity near Hayward. This single locked asperity at depth is also suggested to be extending from Berkeley to Fremont by *Funning et al.* [2005] using a more extensive InSAR data set. Moreover, joint inversion of GPS, InSAR and seismic data sets using an elastic dislocation model reveals two locked patches between depths of 8–12 km located near the southern end of the Hayward fault and between 10 and 30 km distance from Pt. Pinole [*Schmidt et al.*, 2005].

The creeping behavior of the Hayward Fault also varies in time, mainly due to the perturbation of the regional stress field induced by seismic events, such as the 1989 Loma Prieta earthquake [*Lienkaemper et al.*, 1997]. Following this event, surface creeps on the southern Hayward fault slowed down and stopped on one segment, for about six years. In February of 1996, the quiescence was ended by a rapid creep event of 25-30 mm followed by a slow recovery phase, and surface creep rates are only then approaching the pre-Loma Prieta rate [*Lienkaemper et al.*, 2012]. Using the concept of spring-slider and implementing a rate- and state-dependent friction framework through boundary element modeling, *Kanu and Johnson* [2011] suggest that this creep event extended to a depth of ~4 - 7.5 km. *Lienkaemper et al.* [2012] report on another slow slip event at km ~20 - 35 from Point Pinole following the 2007 Oakland Mw 4.2 earthquake. This event continued for several days and was characterized by a logarithmic decay of slip over ~100 days [*Lienkaemper et al.*, 2012].

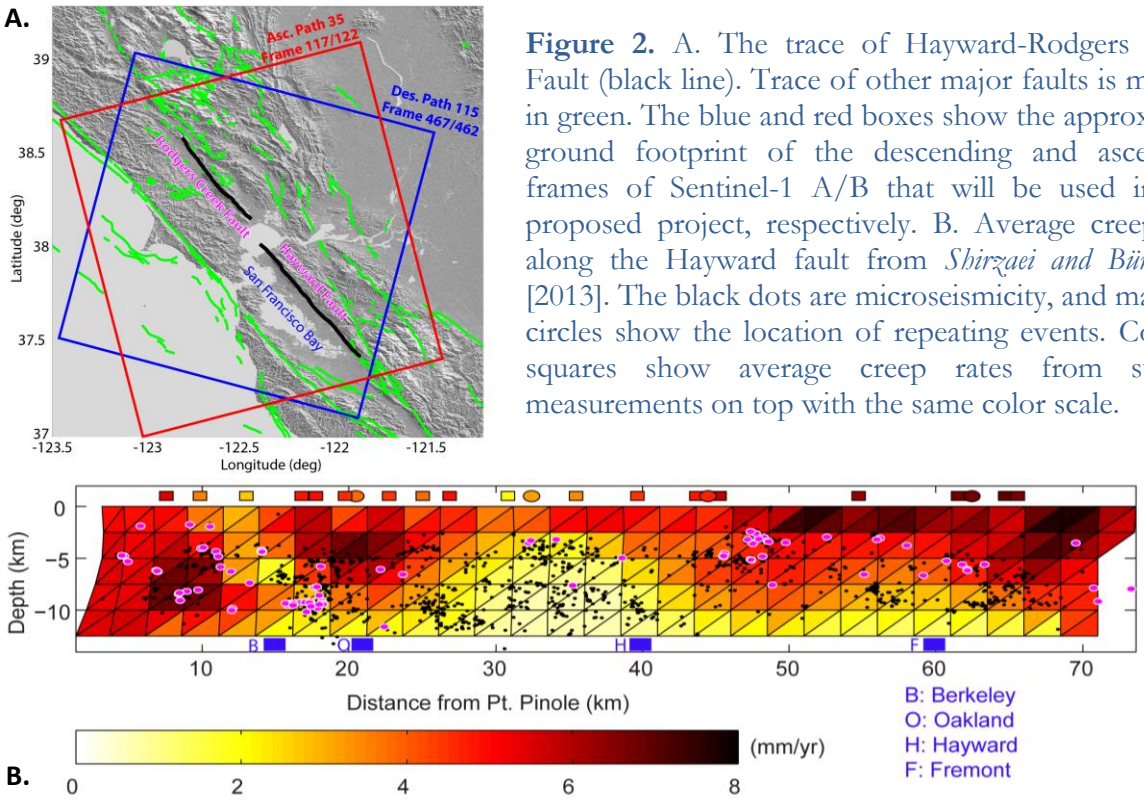


**Figure 2.** A. The trace of Hayward-Rodgers Creek Fault (black line). Trace of other major faults is marked in green. The blue and red boxes show the approximate ground footprint of the descending and ascending frames of Sentinel-1 A/B that will be used in this proposed project, respectively. B. Average creep rate along the Hayward fault from *Shirzaei and Bürgmann* [2013]. The black dots are microseismicity, and magenta circles show the location of repeating events. Colored squares show average creep rates from surface measurements on top with the same color scale.

To solve for the time-dependent model of creep on the Hayward Fault, *Shirzaei and Bürgmann* [2013] inverted 18 years of surface deformation data (1992 - 2010), obtained by interferometric processing of 52 and 50 synthetic aperture radar (SAR) images acquired by the ERS1/2 and Envisat satellites, respectively, and surface creep data obtained at 19 alignments and four creepmeter stations. Their time-dependent model constrains a zone of high slip deficit (low creep rate) that may represent the locked rupture asperity of past and future M≈7 earthquakes (Fig. 2B). They also resolve the source areas of the February 1996 and July 2007 slow-slip events. They identify several additional temporal variations in creep rate along the Hayward Fault, the most important one being a zone of accelerating slip just to the northwest of the major central locked zone. They find that the fault creep imparts stress on the major locked zone at a rate of ~0.003 MPa/yr in addition to the background loading rates. They estimated that a slip-rate deficit equivalent to Mw 6.3-6.8 has accumulated on the fault, since the last event in 1868.

Unlike the HF, there is no unanimous agreement within the literature regarding the rate and location of the shallow creep on the RCF. According to a recent study based on InSAR, GPS, and alignment array observations, the measured creep on the surface is ~2 mm/yr, varying along the Rodgers Creek Fault, while the estimated long-term rate of creep in the deep zone (depth more than 10 km) is 11.6 ± 0.5 mm/yr [*Xu et al.*, 2018]. On the other hand, using InSAR observation alone, *Funning et al.* [2007] estimated creep rates of 3-7 mm/yr for the shallow 6 km of the RCF. Moreover, the repeating earthquake observation, detected within the shallow 10 km of the RCF, suggest a creep rate of ~2 mm/yr in the central RCF, just north of Santa Rosa, and higher creep rate of ~4 mm/yr in the southern section of the RCF [*Senobari and Funning*, 2019]. The lack of repeating earthquakes on the part of RCF beneath the city of Santa Rosa towards the south, however, might be indicative of a locked asperity in this zone. The presence of such strong asperity is also suggested using Lidar-based generated high-resolution DEM as well as data set provided through gravity, aeromagnetic, and seismic-reflection surveys over RCF [*Hecker et al.*, 2016].

## 3. Tools and Data

For the past 25 years, InSAR measurements have provided tremendous excitement in the geodetic and hazards research communities because of their unparalleled spatial coverage and resolution. InSAR and GPS are complementary in that GPS provides long-term stability, vector displacements, and better temporal coverage as compared to the extensive spatial coverage provided by SAR. Because both GPS and InSAR involve the propagation of electromagnetic signals, they share related path delays through the electrically neutral lower atmosphere. Thus, results from one system are directly relevant to the others [*Tong et al.*, 2014]. In our earlier studies, we developed InSAR time series algorithm to analyze InSAR and GPS data sets and measure surface deformation at unprecedented accuracy and resolution [*Khoshmanesh et al.*, 2015; *Miller and Shirzaei*, 2015; *Shirzaei*, 2013; 2015; *Shirzaei and Bürgmann*, 2013; *Shirzaei et al.*, 2012; *Shirzaei et al.*, 2013; *Shirzaei et al.*, 2014; *Shirzaei et al.*, 2015; *Turner et al.*, 2015; *Weston and Shirzaei*, 2016].

The multitemporal InSAR approaches, include methods using single-master interferometry (e.g., Permanent Scatterer [*Ferretti et al.*, 2001; *Hooper et al.*, 2007]) and methods implementing a multi-master interferometry (e.g. Small Baseline Subset [*Berardino et al.*, 2002], Wavelet-Based InSAR [*Shirzaei*, 2013], multiscale InSAR Time Series [*Hetland et al.*, 2012] and Multitrack Wavelet-Based InSAR [*Shirzaei*, 2015]). One of the benefits of a time series approach is that it readily lends itself to temporal filtering, mitigating the effects of atmospheric noise, which is a significant error source in traditional InSAR. It can also more clearly delineate temporally variable components of the deformation field and improves the time-dependent deformation models. Here, we used a Wavelet Based InSAR (WabInSAR) algorithm to analyze SAR data sets and generate several high-resolution spatiotemporal maps of surface deformation along the HF-RCF system. The accuracy of the results is assessed by comparing them against independent observations such as GPS. Throughout this project we also analyzed, interpreted and integrated other data sets including, creepmeter, alinement array, geology and lithology, seismic velocities, and tomography.

## 4. Models

Here we applied a kinematic modeling scheme to solve for the spatial distribution of creep rate along the HF-RCF system. Starting with a simulated fault geometry using a mesh of triangular (or rectangular) dislocations, the relation between surface observation ($L$) and fault creep ($C$) is as follows;

$$L + v = BC \quad , \quad P = \sigma_0^2 \Sigma_l^{-1}{}_l \qquad (1)$$

where, $B$ is the design matrix, $v$ is observation residual and $\Sigma_l^{-1}{}_l$ is observation variance-covariance matrix. To integrate the CREs into the creep inversion, we consider the following constraint equation;

$$C^{CRE} + \varepsilon = C \quad , \quad P^c = \sigma_0^2 \Sigma_S^{-1}{}_S \qquad (2)$$

where, $C^{CRE}$ is the creep obtained from the CREs, $\varepsilon$ is the vector of residuals and $\Sigma_S^{-1}{}_S$ is the variance-covariance matrix of CRE creep. System of Equations 1 and 2 can be solved using a least-squares optimization technique, subject to some smoothing criteria [*Shirzaei and Bürgmann*, 2013]. Despite the advantages of gradient-based least squares optimization methods for solving various problems [*Lawson and Hanson*, 1974; *Mikhail and Ackermann*, 1982; *Segall*, 2010; *Tarantola*, 1987], they are less effective to account for the effect of various apriori information as well as observation and model errors. Hence to obtain a probabilistic estimate of the creep and full variance-covariance matrices, a Bayesian optimization framework is applied. Bayesian inversion is widely used for modeling volcanic and tectonic processes (e.g. [*Anderson and Segall*, 2013; *Fukuda and Johnson*, 2008;

*Fukuda and Johnson*, 2010; *Jolivet et al.*, 2015; *Minson et al.*, 2013; *Minson et al.*, 2014; *Murray et al.*, 2014; *Rousset et al.*, 2016]). Bayesian inference is the process of analyzing statistical models with the incorporation of prior knowledge about the model or model parameters [*Kaipio and Somersalo*, 2006]. The root of such inference is Bayes' theorem:

$$P(parameters|data) = \frac{P(data|parameetrs)}{P(data)} \alpha\ likelihood\ \times\ prior \quad (3)$$

Where P() is the probability function. Suppose we have normally distributed observations, $X|\theta \sim N(\theta, \sigma^2)$, where sigma is known and the prior distribution for theta is $\theta \sim N(\mu, \tau^2)$. Also, $\mu$ and $\tau$ are known. If we observe n samples of X, we can obtain the posterior distribution for $\theta$ [*Kaipio and Somersalo*, 2006] as:

$$\theta|X \sim N\left(\frac{\tau^2}{\sigma^2/2+\tau^2}\overline{X} + \frac{\sigma^2/2}{\sigma^2/2+\tau^2}\mu, \frac{(\sigma^2/2)\tau^2}{\sigma^2/2+\tau^2}\right) \quad , \quad \overline{X} = \frac{1}{n}\sum_{i=1}^{n} X_i \quad (4)$$

Markov Chain Monte Carlo (MCMC) sampling was used to characterize the posterior probability distributions [*Metropolis et al.*, 1953; *Mosegaard and Tarantola*, 1995].

## 5. Results and conclusions

Our SAR dataset includes ~200 images acquired by Sentinel-1A/B C-Band satellite in descending and ascending viewing geometries during 2014 and 2019. We also incorporate 120 sequences of CREs with data from 5 creepmeters in our analysis. Figure 3 shows the obtained surface deformation velocity maps for each viewing geometries.

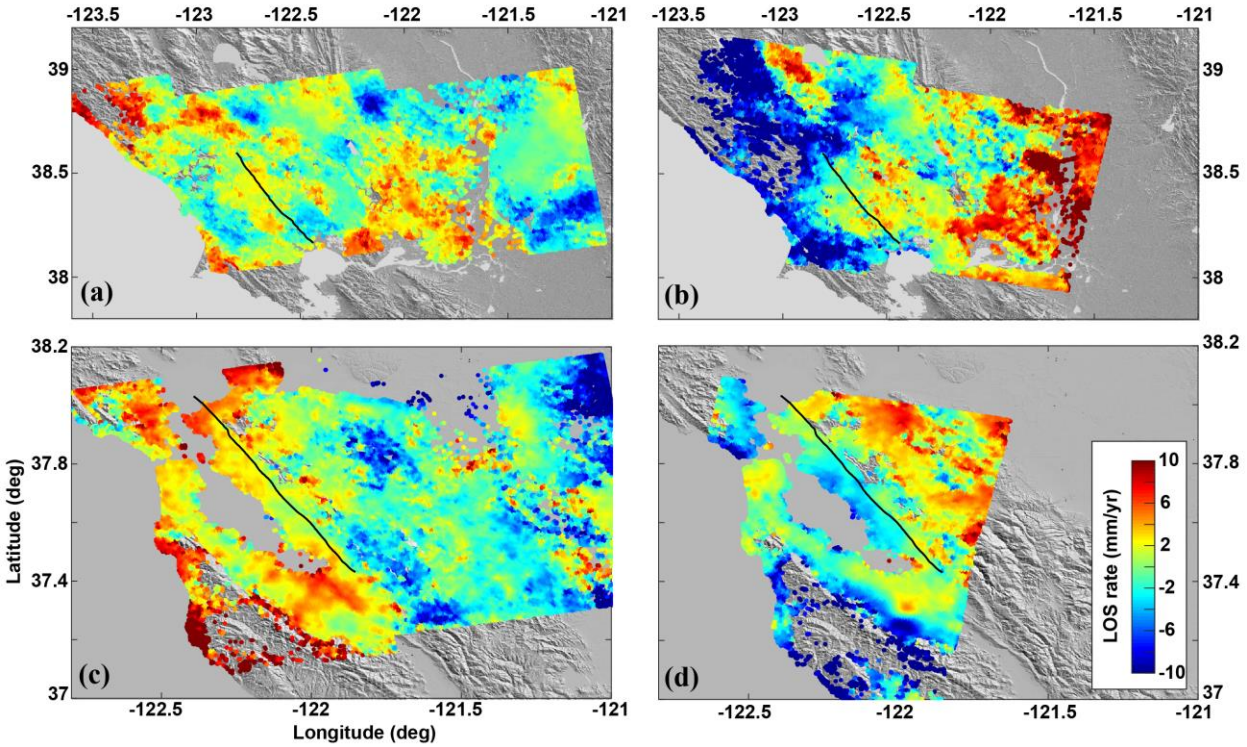


**Figure 3.** Long-term LOS deformation rates during 2014-2019: (a) Ascending rates along RCF, (b) Descending rates along RCF, (c) Ascending rates along HF, and (d) Descending rates along HF, (Khoshmanesh et al. 2020, in prep).

Availability of the LOS velocities in ascending and descending viewing geometry allows solving for the vertical and east-west displacement components, assuming that the contribution from the north component is negligible due to polar-orbiting SAR satellites. Figure 4 shows the spatial distribution of the obtained vertical deformation rate. The majority of the observed vertical land motion is attributed to hydrological processes and sediment compaction. Using this vertical rate, we correct the LOS velocity obtained in descending viewing geometry.

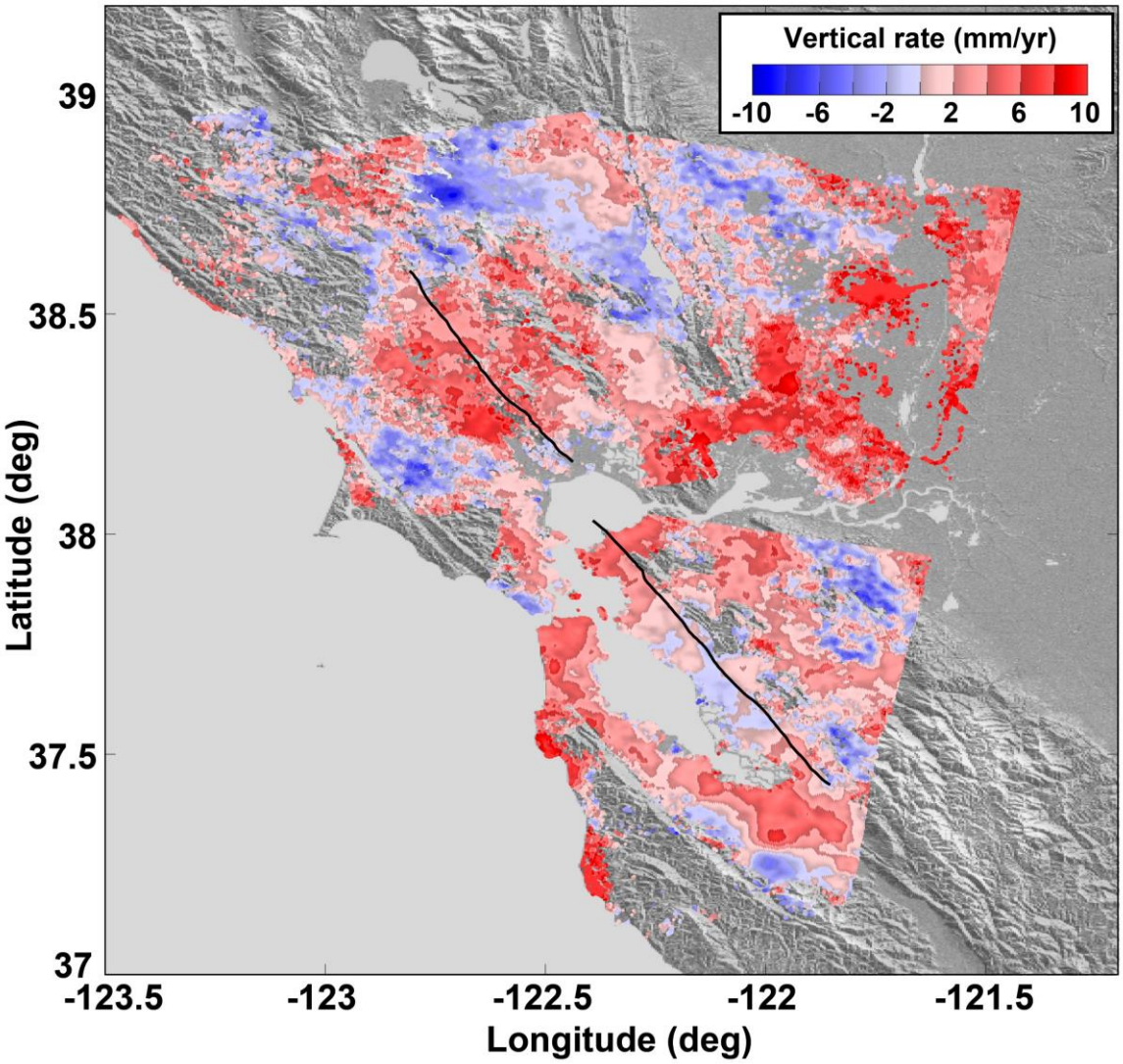


Figure 4. Long-term vertical land deformation rate during 2014-2019

Figure 5a shows the LOS velocity field in descending orbit geometry corrected for vertical motions alongside the GPS velocities. The rectangles denote the location of the GPS stations, which are color-coded based on the GPS 2D velocities projected into the LOS direction. The black arrows show the horizontal velocity of the GPS stations. Visual comparison of the InSAR LOS velocity and projected GPS velocities shows a good agreement between these two independent datasets. The difference between the GPS and InSAR LOS velocity has an average of -0.3 mm/yr and a standard deviation of ~2 mm/yr (inset in Figure 5a). The trace of the HF and RCF roughly defines the boundary between the red and blue areas in Figure 5a, which correspond to the movement toward and away from the satellite, respectively. The LOS velocities along Two profiles across the HF and

RCF are shown in Figure 5b. The corresponding amount of surface deformation measured by the GPS stations (red dots), with errorbars showing 1 mm/yr uncertainty, are also shown alongside the InSAR observations further to validate the implemented method for InSAR data processing. As seen, there is a good agreement between InSAR and GPS observations within the study area.

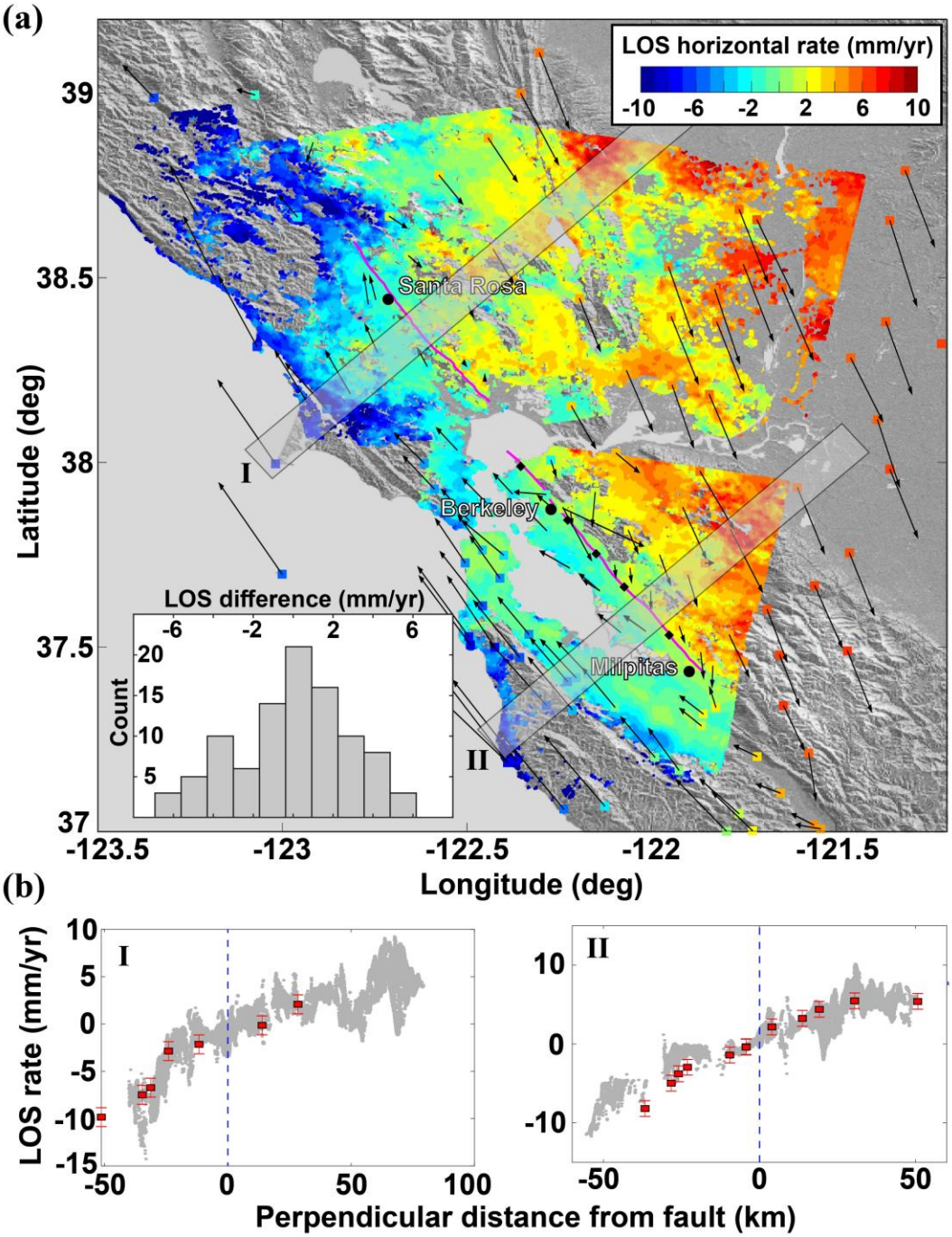


**Figure 5. Long-term horizontal deformation rate during 2014-2019:** (**a**) Descending InSAR observations along both HF and RCF after removing the contributions from vertical land motion, along with the GPS horizontal rates, and (**b**) GPS (red) versus InSAR (gray) along the two profiles perpendicular to the fault trace shown in (a).

Applying the inversion scheme detailed above to the LOS deformation rate shown in Figure 5a, we solve for the spatiotemporal distribution of the creep along the HF-RCF system. Figure 6 shows the 3D perspective of the obtained HF-RCF creep rate. The model along HF is characterized by a deep creeping patch at a rate of 9 mm/yr near its south, a central locked patch, and a shallow creeping zone at a rate of 6 mm/yr near its north. Along the RCF, the majority of fast creeping zones are deep below 5 km. The only shallow creeping zone is located north of sears point, which creeps at a rate of ~6 mm/y. we further overlay the extent of the HF central locked zone that is obtained by *Shirzaei and Bürgmann* [2013]. Interestingly, we find that the area of the locked patch obtained here is slightly larger than that of the earlier study. Further works need to be done to investigate whether this difference is statistically significant. Additionally, we estimated that HF alone accumulates a seismic moment (Mw) of 5.2 – 5.5 each year. This estimate for RCF is 5.0 – 5.4, while the combined system accumulates seismic moment at the rate of 5.4 – 5.7 per year.

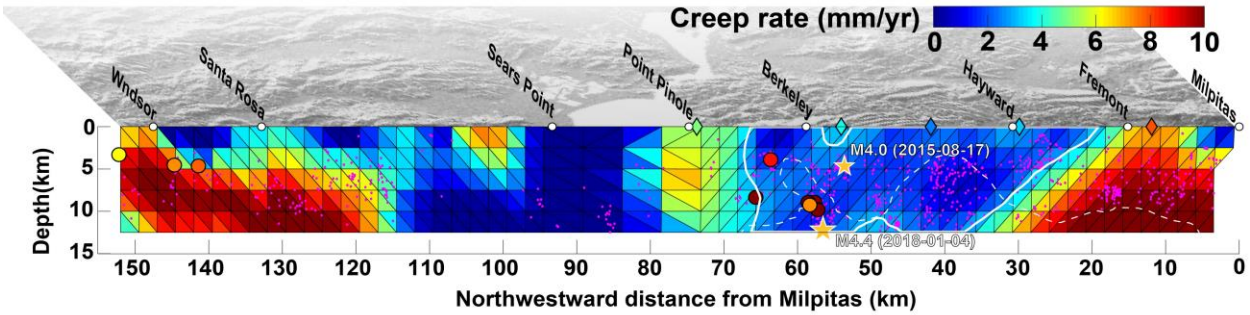


Figure 6. Long-term creep rate during 2014-2019 on HF and RCF: diamonds show the creepmeter stations, solid circles show the detected CRE sequences, and magenta dots show the microseismicity. Solid and dashed white contour denote the limit of the locked asperity on HF obtained in this study and that in Shirzaei and Burgmann (2013, JGR), respectively, showing that the locked area has grown in size.

## Acknowledgment

This study was funded by the United States Geological Survey grant G18AP00008. The European Space Agency provided radar data. GPS data are obtained from the Plate Boundary Observatory, a component of EarthScope, operated by UNAVCO and funded by the National Science Foundation. Taka'aki Taira provided the repeating earthquakes.

## References

Anderson, K., and P. Segall (2013), Bayesian inversion of data from effusive volcanic eruptions using physics-based models: Application to Mount St. Helens 2004-2008, *Journal of Geophysical Research-Solid Earth*, *118*(5), 2017-2037, doi:10.1002/jgrb.50169.

Avouac, J.-P. (2015), From Geodetic Imaging of Seismic and Aseismic Fault Slip to Dynamic Modeling of the Seismic Cycle, in *Annual Review of Earth and Planetary Sciences, Vol 43*, edited by R. Jeanloz and K. H. Freeman, pp. 233-271, doi:10.1146/annurev-earth-060614-105302.

Berardino, P., G. Fornaro, R. Lanari, and E. Sansosti (2002), A new algorithm for surface deformation monitoring based on small baseline differential SAR interferograms, *IEEE Transactions on Geosciences and Remote Sensing*, *40*(11), 2375-2383.

Bürgmann, R., D. Schmidt, R. M. Nadeau, M. d'Alessio, E. Fielding, D. Manaker, T. V. McEvilly, and M. H. Murray (2000), Earthquake potential along the northern Hayward fault, California, *Science*, *289*(5482), 1178-1182.

Chlieh, M., P. A. Mothes, J. M. Nocquet, P. Jarrin, P. Charvis, D. Cisneros, Y. Font, J. Y. Collot, J. C. Villegas-Lanza, F. Rolandone, M. Vallee, M. Regnier, M. Segovia, X. Martin, and H. Yepes (2014), Distribution of discrete seismic asperities and aseismic slip along the Ecuadorian megathrust, *Earth and Planetary Science Letters*, *400*, 292-301, doi:10.1016/j.epsl.2014.05.027.

Cho, I., T. Tada, and Y. Kuwahara (2009), Stress triggering of large earthquakes complicated by transient aseismic slip episodes, *Journal of Geophysical Research-Solid Earth*, *114*, doi:10.1029/2008jb006125.

d'Alessio, M. A., I. A. Johanson, R. Burgmann, D. A. Schmidt, and M. H. Murray (2005), Slicing up the San Francisco Bay Area: block kinematics and fault slip rates from GPS-derived surface velocities, *Journal of Geophysical Research-Solid Earth*, *110*(B6).

Dieterich, J. H. (1978), Time-dependent friction and the mechanics of stick slip, *Pageoph*, *116*, 790-806.

Evans, E. L., J. P. Loveless, and B. J. Meade (2012), Geodetic constraints on San Francisco Bay Area fault slip rates and potential seismogenic asperities on the partially creeping Hayward fault, *Journal of Geophysical Research-Solid Earth*, *117*.

Ferretti, A., C. Prati, and F. Rocca (2001), Permanent scatterers in SAR interferometry, *IEEE transactions on geoscience and remote sensing*, *39*, 8-20

Field, E. H., G. P. Biasi, P. Bird, T. E. Dawson, K. R. Felzer, D. D. Jackson, K. M. Johnson, T. H. Jordan, C. Madden, A. J. Michael, K. R. Milner, M. T. Page, T. Parsons, P. M. Powers, B. E. Shaw, W. R. Thatcher, R. J. Weldon, II, and Y. Zeng (2015), Long-Term Time-Dependent Probabilities for the Third Uniform California Earthquake Rupture Forecast (UCERF3), *Bulletin of the Seismological Society of America*, *105*(2A), 511-543, doi:10.1785/0120140093.

Fukuda, J., and K. M. Johnson (2008), A Fully Bayesian Inversion for Spatial Distribution of Fault Slip with Objective Smoothing, *Bulletin of the Seismological Society of America*, *98*(3), 1128-1146, doi:10.1785/0120070194.

Fukuda, J. i., and K. M. Johnson (2010), Mixed linear-non-linear inversion of crustal deformation data: Bayesian inference of model, weighting and regularization parameters, *Geophysical Journal International*, *181*(3), 1441-1458, doi:10.1111/j.1365-246X.2010.04564.x.

Funning, G., R. Bürgmann, A. Ferretti, F. Novali, and D. A. Schmidt (2005), Kinematics, asperities and seismic potential of the Hayward fault, California from ERS and RADARSAT PS-InSAR, *EOS, Transactions American Geophysical Union*, *86*(52).

Funning, G. J., R. Bürgmann, A. Ferretti, F. Novali, and A. Fumagalli (2007), Creep on the Rodgers Creek fault, northern San Francisco Bay area from a 10 year PS-InSAR dataset, *Geophys. Res. Lett.*, *34*(19), doi:10.1029/2007gl030836.

Hecker, S., V. E. Langenheim, R. A. Williams, C. S. Hitchcock, and S. B. DeLong (2016), Detailed Mapping and Rupture Implications of the 1 km Releasing Bend in the Rodgers Creek Fault at Santa Rosa, Northern CaliforniaDetailed Mapping and Rupture Implications of the 1 km Releasing Bend in the RCF at Santa Rosa, *Bulletin of the Seismological Society of America*, *106*(2), 575-594, doi:10.1785/0120150152.

Hetland, E. A., P. Muse, M. Simons, Y. N. Lin, P. S. Agram, and C. J. DiCaprio (2012), Multiscale InSAR Time Series (MInTS) analysis of surface deformation, *Journal of Geophysical Research-Solid Earth*, *117*, doi:10.1029/2011jb008731.

Hooper, A., P. Segall, and H. Zebker (2007), Persistent scatterer interferometric synthetic aperture radar for crustal deformation analysis, with application to Volcan Alcedo, Galapagos, *Journal of Geophysical Research-Solid Earth*, *112*(B7), doi:Doi 10.1029/2006jb004763.

Jolivet, R., M. Simons, P. S. Agram, Z. Duputel, and Z. K. Shen (2015), Aseismic slip and seismogenic coupling along the central San Andreas Fault, *Geophysical Research Letters*, *42*(2), 297-306, doi:10.1002/2014gl062222.

Kaipio, J., and E. Somersalo (2006), *Statistical and computational inverse problems*, Springer Science & Business Media.

Kaneko, Y., J.-P. Avouac, and N. Lapusta (2010), Towards inferring earthquake patterns from geodetic observations of interseismic coupling, *Nature Geoscience*, *3*(5), 363-U324, doi:10.1038/ngeo843.

Kanu, C., and K. Johnson (2011), Arrest and recovery of frictional creep on the southern Hayward fault triggered by the 1989 Loma Prieta, California, earthquake and implications for future earthquakes, *Journal of Geophysical Research-Solid Earth*, *116*.

Kato, A., K. Obara, T. Igarashi, H. Tsuruoka, S. Nakagawa, and N. Hirata (2012), Propagation of Slow Slip Leading Up to the 2011 M-w 9.0 Tohoku-Oki Earthquake, *Science*, *335*(6069), 705-708.

Kawasaki, I., Y. Asai, and Y. Tamura (2001), Space-time distribution of interplate moment release including slow earthquakes and the seismo-geodetic coupling in the Sanriku-oki region along the Japan trench, *Tectonophysics*, *330*(3-4), 267-283, doi:10.1016/s0040-1951(00)00245-6.

Khoshmanesh, M., M. Shirzaei, and R. M. Nadeau (2015), Time-dependent model of aseismic slip on the Central San Andreas Fault from InSAR time series and repeating earthquakes, *J. Geophys. Res. Solid Earth*, *120*, doi:10.1002/2015JB012039.

Lawson, C. L., and R. J. Hanson (1974), *Solving Least Squares Problems*, Prentice Hall, Englewood Cliffs, New Jersey, 340 pp.

Lienkaemper, J. J., G. Borchardt, and M. Lisowski (1991), Historic creep rate and potential for seismic slip along the Hayward Fault, California, *J. Geophys. Res.*, *96*, 18261-18283.

Lienkaemper, J. J., and J. Galehouse (1998), New evidence doubles the seismic potential of the Hayward fault, *Seismol. Res. Lett*, *69*, 519– 523.

Lienkaemper, J. J., J. S. Galehouse, and R. W. Simpson (1997), Creep response of the Hayward fault to stress changes caused by the Loma Prieta earthquake, *Science*, *276*(5321), 2014-2016.

Lienkaemper, J. J., F. S. McFarland, R. W. Simpson, R. G. Bilham, D. A. Ponce, J. J. Boatwright, and S. J. Caskey (2012), Long-Term Creep Rates on the Hayward Fault: Evidence for Controls on the Size and Frequency of Large Earthquakes, *Bulletin of the Seismological Society of America*, *102*(1), 31-41.

Lienkaemper, J. J., P. L. Williams, and T. P. Guilderson (2010), Evidence for a Twelfth Large Earthquake on the Southern Hayward Fault in the Past 1900 Years, *Bulletin of the Seismological Society of America*, *100*(5A), 2024-2034.

Metropolis, N., M. N. Rosenbluth, A. W. Rosenbluth, A. H. Teller, and E. Teller (1953), Equation of state calculations by fast computing machines, *Journal of Chemical Physics*, *21*(6), 1087–1092.

Mikhail, E. M., and F. E. Ackermann (1982), *Observations and least squares*, University Press of America.

Miller, M. M., and M. Shirzaei (2015), Spatiotemporal characterization of land subsidence and uplift in Phoenix using InSAR time series and wavelet transforms *J. Geophys. Res. Solid Earth*, *120*, doi:10.1002/2015JB012017.

Minson, S. E., M. Simons, and J. L. Beck (2013), Bayesian inversion for finite fault earthquake source models I-theory and algorithm, *Geophysical Journal International*, *194*(3), 1701-1726, doi:10.1093/gji/ggt180.

Minson, S. E., M. Simons, J. L. Beck, F. Ortega, J. Jiang, S. E. Owen, A. W. Moore, A. Inbal, and A. Sladen (2014), Bayesian inversion for finite fault earthquake source models - II: the 2011 great Tohoku-oki, Japan earthquake, *Geophysical Journal International*, *198*(2), 922-940, doi:10.1093/gji/ggu170.

Mosegaard, K., and A. Tarantola (1995), Monte Carlo sampling of solutions to inverse problems, *J. Geophys. Res.*, *100*, 12431-12448.

Murray, J. R., S. E. Minson, and J. L. Svarc (2014), Slip rates and spatially variable creep on faults of the northern San Andreas system inferred through Bayesian inversion of Global Positioning System data, *Journal of Geophysical Research-Solid Earth*, *119*(7), 6023-6047, doi:10.1002/2014jb010966.

Pacheco, J. F., L. R. Sykes, and C. H. Scholz (1993), NATURE OF SEISMIC COUPLING ALONG SIMPLE PLATE BOUNDARIES OF THE SUBDUCTION TYPE, *Journal of Geophysical Research-Solid Earth*, *98*(B8), 14133-14159, doi:10.1029/93jb00349.

Perfettini, H., J. P. Avouac, H. Tavera, A. Kositsky, J. M. Nocquet, F. Bondoux, M. Chlieh, A. Sladen, L. Audin, D. L. Farber, and P. Soler (2010), Seismic and aseismic slip on the central Peru megathrust, *Nature*, *465*(7294), 78-81, doi:10.1038/nature09062.

Radiguet, M., H. Perfettini, N. Cotte, A. Gualandi, B. Valette, V. Kostoglodov, T. Lhomme, A. Walpersdorf, E. C. Cano, and M. Campillo (2016), Triggering of the 2014 Mw7. 3 Papanoa earthquake by a slow slip event in Guerrero, Mexico, *Nature Geoscience*, *9*(11), 829-833.

Rousset, B., R. Jolivet, M. Simons, C. Lasserre, B. Riel, P. Milillo, Z. Cakir, and F. Renard (2016), An aseismic slip transient on the North Anatolian Fault, *Geophysical Research Letters*, *43*(7), 3254-3262, doi:10.1002/2016gl068250.

Ruina, A. (1983), Slip instability and state variable friction laws, *J. Geophys. Res.*, *88*(B12), 10359-10370.

Savage, J. C., and M. Lisowski (1993), Inferred Depth of Creep on the Hayward Fault, Central California, *Journal of Geophysical Research-Solid Earth*, *98*(B1), 787-793.

Schmidt, D. A., R. Bürgmann, R. M. Nadeau, and M. d'Alessio (2005), Distribution of aseismic slip rate on the Hayward fault inferred from seismic and geodetic data, *J. Geophys. Res.*, *110*(B8), doi:doi: 10.1029/2004JB003397.

Schurr, B., G. Asch, S. Hainzl, J. Bedford, A. Hoechner, M. Palo, R. Wang, M. Moreno, M. Bartsch, Y. Zhang, O. Oncken, F. Tilmann, T. Dahm, P. Victor, S. Barrientos, and J.-P. Vilotte (2014), Gradual unlocking of plate boundary controlled initiation of the 2014 Iquique earthquake, *Nature*, *512*(7514), 299-302, doi:10.1038/nature13681.

Segall, P. (2010), *Earthquake and Volcano Deformation*, 458 pp., Princeton University Press.

Senobari, N. S., and G. Funning (2019), Widespread fault creep in the northern San Francisco Bay Area revealed by multi-station cluster detection of repeating earthquakes, *Earth and Space Science Open Archive*, doi:doi:10.1002/essoar.10500868.1.

Shirzaei, M. (2013), A Wavelet-Based Multitemporal DInSAR Algorithm for Monitoring Ground Surface Motion, *Ieee Geoscience and Remote Sensing Letters*, *10*(3), 456-460, doi:Doi 10.1109/Lgrs.2012.2208935.

Shirzaei, M. (2015), A seamless multitrack multitemporal InSAR algorithm, *Geochem. Geophys. Geosyst.*, *16*, doi:10.1002/2015GC005759.

Shirzaei, M., and R. Bürgmann (2013), Time-dependent model of creep on Hayward fault inferred from joint inversion of 18 years InSAR time series and surface creep data, *J. Geophys. Res. Solid Earth*, *118*( 1733–1746), doi:10.1002/jgrb.50149.

Shirzaei, M., R. Bürgmann, O. Oncken, T. R. Walter, P. Victor, and O. Ewiak (2012), Response of forearc crustal faults to the megathrust earthquake cycle: InSAR evidence from Mejillones Peninsula, Northern Chile, *Earth and Planetary Science Letters*, *333*, 157-164, doi:DOI 10.1016/j.epsl.2012.04.001.

Shirzaei, M., R. Bürgmann, and T. Taira (2013), Implications of recent asperity failures and aseismic creep for time-dependent earthquake hazard on the Hayward fault, *Earth and Planetary Science Letters*, *371–372*(0), 59-66, doi:http://dx.doi.org/10.1016/j.epsl.2013.04.024.

Shirzaei, M., R. Bürgmann, N. Uchida, Y. Hu, F. Pollitz, and T. Matsuzawa (2014), Seismic versus aseismic slip: Probing mechanical properties of the northeast Japan subduction zone, *Earth and Planetary Science Letters*, *406*, 7-13, doi:10.1016/j.epsl.2014.08.035.

Shirzaei, M., M. L. Rudolph, and M. Manga (2015), Deep and shallow sources for the Lusi mud eruption revealed by surface deformation, *Geophys. Res. Lett.*, *42*, doi:10.1002/2015GL064576.

Simpson, R. W., J. J. Lienkaemper, and J. S. Galehouse (2001), Variations in creep rate along the Hayward Fault, California, interpreted as changes in depth of creep, *Geophysical Research Letters*, *28*(11), 2269-2272.

Tarantola, A. (1987), *Inverse Problem Theory - Methods for Data Fitting and Model Parameter Estimation*, Elsevier, Amsterdam, 613 pp.

Tong, X., B. Smith-Konter, and D. T. Sandwell (2014), Is there a discrepancy between geological and geodetic slip rates along the San Andreas Fault System?, *Journal of Geophysical Research-Solid Earth*, *119*(3), 2518-2538, doi:10.1002/2013jb010765.

Toppozada, T. R., and G. Borchardt (1998), Re-evaluation of the 1836 "Hayward fault" and the 1838 San Andreas fault earthquakes, *Bulletin of the Seismological Society of America*, *88*(1), 140-159.

Turner, R. C., M. Shirzaei, R. M. Nadeau, and R. Bürgmann (2015), Slow and Go: Pulsing Slip Rates on the Creeping Section of the San Andreas Fault, *J. Geophys. Res. Solid Earth*, *120*, doi:10.1002/2015JB011998.

Uchida, N., T. Iinuma, R. M. Nadeau, R. Buergmann, and R. Hino (2016), Periodic slow slip triggers megathrust zone earthquakes in northeastern Japan, *Science*, *351*(6272), 488-492, doi:10.1126/science.aad3108.

Wallace, L. M., J. Beavan, S. Bannister, and C. Williams (2012), Simultaneous long-term and short-term slow slip events at the Hikurangi subduction margin, New Zealand: Implications for processes that control slow slip event occurrence, duration, and migration, *Journal of Geophysical Research-Solid Earth*, *117*, doi:10.1029/2012jb009489.

Watt, J., D. Ponce, T. Parsons, and P. Hart (2016), Missing link between the Hayward and Rodgers Creek faults, *Science advances*, *2*(10), e1601441.

Weston, J., and M. Shirzaei (2016), Combining GPS and repeating earthquakes for a high resolution analysis of subduction zone coupling, *Tectonophysics*, *667*, 37-47.

Wyss, M. (2001), Locked and creeping patches along the Hayward Fault, California, *Geophys. Res. Lett.*, *28*(18), 3537-3540.

Xu, W., S. Wu, K. Materna, R. Nadeau, M. Floyd, G. Funning, E. Chaussard, C. W. Johnson, J. R. Murray, X. Ding, and R. Bürgmann (2018), Interseismic Ground Deformation and Fault Slip Rates in the Greater San Francisco Bay Area From Two Decades of Space Geodetic Data, *J. Geophys. Res.*, *123*(9), 8095-8109, doi:10.1029/2018jb016004.